Electronic Supplementary Information

Constructing New Metal-Organic Frameworks with Complicated Ligands Generated from "One-Pot" In Situ Reactions

Xiang-Jing Kong, Tao He, Yong-Zheng Zhang, Xue-Qian Wu, Si-Nan Wang, Ming-Ming Xu, Guang-Rui Si, and Jian-Rong Li*

Beijing Key Laboratory for Green Catalysis and Separation, Department of Chemistry and Chemical Engineering, College of Environmental and Energy Engineering, Beijing University of Technology, Beijing 100124, P. R. China.

E-mail: jrli@bjut.edu.cn

Contents

S1. Materials and instruments

All reagents and solvents (AR grade) were commercially purchased and used as received. ^{1}H NMR data were collected on a BRUKER AVANCE III HD 400M NMR spectrometer. FT-IR spectra were recorded on an IRAffinity-1 instrument. TGA data were obtained on a TGA-50 (SHIMADZU) thermogravimetric analyzer with a heating rate of 10 °C min^{-1} under air atmosphere. The powder X-ray diffraction (PXRD) patterns were recorded on a BRUKER D8-Focus Bragg-Brentano X-ray Powder Diffractometer equipped with a Cu sealed tube (λ = 1.54178) at room temperature. Simulation of the PXRD patterns was carried out by the single-crystal data and diffraction-crystal module of the Mercury program available free of charge via internet at https://www.ccdc.cam.ac.uk/. Gas adsorption-desorption isotherms were obtained using a Micrometrics ASAP 2020.

S2. Ligand scope and synthesis

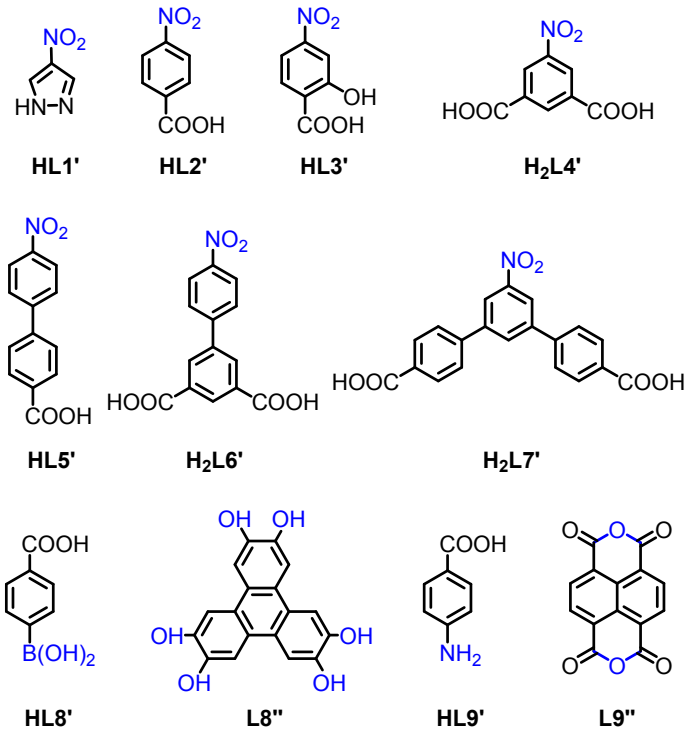

Fig. S1 The ligand scope in present work.

Synthesis of H_2L6'

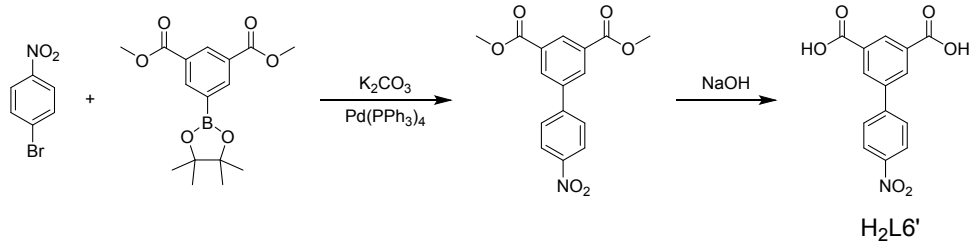

Scheme S1 Synthesis of H_2L6'.

To a solution of 1-bromo-4-nitrobenzene (5.0 g, 24.8 mmol), dimethyl 5-(4,4,5,5-tetramethyl-1,3,2-dioxaborolan-2-yl)isophthalate (9.5 g, 29.7 mmol) and K_2CO_3 (5.1 g, 37.1 mmol) in 1,2-dimethoxyethane (DME, 120 mL) and H_2O (30 mL) $Pd(PPh_3)_4$ (1.4 g, 1.2 mmol) was added under nitrogen atmosphere. The resulting mixture was stirred at refluxing temperature. After 24 h the resulting yellow suspension was cooled to room temperature and a precipitate was filtered off. The solid was washed with water (50 mL × 3), and then with EtOH (50 mL × 3). Drying on the air resulted dimethyl 4'-nitro-[1,1'-biphenyl]-3,5-dicarboxylate (5.3 g, 67.9%) as a yellow powder.

To a solution of dimethyl 4'-nitro-[1,1'-biphenyl]-3,5-dicarboxylate (5.3 g, 16.8 mmol) in THF (50 mL), MeOH (50 mL) and H_2O (50 mL) was added NaOH (2.7 g, 67.2 mmol). The resulting mixture was stirred at 70 °C for 24 h. After evaporation of THF and MeOH, the aqueous residue was acidified with 2 M HCl to pH = 3. The resulting precipitate was filtered and washed with H_2O (40 mL × 3) and then MeOH (40 mL × 3). The solid was dried at 60 °C in vacuum to give 4'-nitro-[1,1'-biphenyl]-3,5-dicarboxylic acid as a yellow solid (4.3 g, 89.1%).

Synthesis of H_2L7'

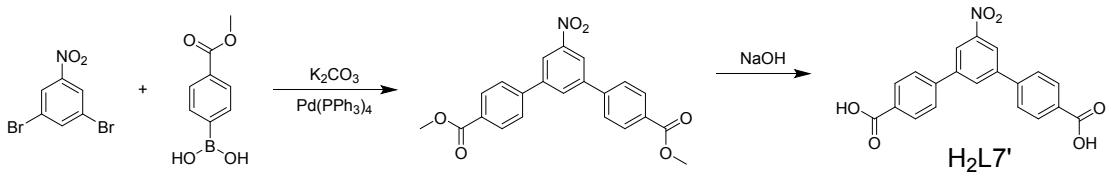

Scheme S2 Synthesis of H_2L7'.

To a solution of 1,3-dibromo-5-nitrobenzene (5.0 g, 17.8 mmol), (4-

(methoxycarbonyl)phenyl)boronic acid (9.6 g, 53.4 mmol) and K_2CO_3 (9.8 g, 71.2 mmol) in 1,2-dimethoxyethane (DME, 120 mL) and H_2O (30 mL) $Pd(PPh_3)_4$ (1.0 g, 0.9 mmol) was added under nitrogen atmosphere. The resulting mixture was stirred at refluxing temperature. After 36 h resulting yellow suspension was cooled to room temperature and a precipitate was filtered off. The solid was washed with water (50 mL × 3), and then with EtOH (50 mL × 3). Drying on the air resulted dimethyl 5'-nitro-[1,1':3',1"-terphenyl]-4,4"-dicarboxylate (5.1 g, 73.2%) as a yellow powder.

To a solution of dimethyl 4'-nitro-[1,1'-biphenyl]-3,5-dicarboxylate (5.1 g, 13.0 mmol) in THF (50 mL), MeOH (50 mL) and H_2O (50 mL) was added NaOH (2.1 g, 52.1 mmol). The resulting mixture was stirred at 70 °C for 24 h. After evaporation of THF and MeOH, the aqueous residue was acidified with 2 M HCl to pH = 3. The resulting precipitate was filtered and washed with H_2O (50 mL × 3) and then MeOH (50 mL × 3). The solid was dried at 60 °C in vacuum to give 5'-nitro-[1,1':3',1"-terphenyl]-4,4"-dicarboxylic acid H_2L7' as a yellow solid (3.5 g, 73.9%).

S3. MOF synthesis

Synthesis of BUT-101

$Cu(NO_3)_2 \cdot 3H_2O$ (0.02 mmol, 5 mg) and H_2L6' (0.01 mmol, 3 mg) were ultrasonically dissolved in 1 mL of DMA. To the solution in a 4 mL glass vial were added 0.2 mL of deionized water. The vial was sealed and then heated at 80 °C for 24 h in an oven. After cooling to room temperature, the blue rod-like crystals of BUT-101(Cu) [$(Cu(L6)(H_2O)_2)$] were collected by filtration, and washed with DMA and acetone. Yield 2.9 mg (78% based on H_2L6' ligand).

$Zn(NO_3)_2 \cdot 6H_2O$ (0.02 mmol, 6 mg) and H_2L6' (0.01 mmol, 3 mg) were ultrasonically dissolved in 1 mL of DMF. To the solution in a 4 mL glass vial were added 0.5 mL of methanol. The vial was sealed and then heated at 80 °C for 48 h in an oven. After cooling to room temperature, the yellow block crystals of BUT-101(Zn) [$Zn(L6)(H_2O)_2$] were collected by filtration, and washed with DMF and acetone.

Yield 2.6 mg (70% based on H_2L6' ligand).

Synthesis of BUT-102

$Cd(NO_3)_2 \cdot 4H_2O$ (0.02 mmol, 6 mg) and H_2L6' (0.01 mmol, 3 mg) were ultrasonically dissolved in 1 mL of DMF. To the solution in a 4 mL glass vial were added 0.3 mL of methanol and 1 mL of deionized water. The vial was sealed and then heated at 70 °C for 24 h in an oven. After cooling to room temperature, the lamellar crystals of BUT-102 [$Cd(L6)(H_2O)$] were collected by filtration, and washed with DMF and acetone. Yield 2.5 mg (62% based on H_2L6' ligand).

Synthesis of BUT-103

$MnCl_2 \cdot 4H_2O$ (0.02 mmol, 4 mg) and H_2L6' (0.01 mmol, 3 mg) were ultrasonically dissolved in 1 mL of DMF. To the solution in a 4 mL glass vial were added 0.25 mL of ethanol. The vial was sealed and then heated at 90 °C for 40 h in an oven. After cooling to room temperature, the yellow block crystals of BUT-103 $[Mn_4(L6)_4(DMF)_6] \cdot (DMF)_3$ were collected by filtration, and washed with DMF and acetone. Yield 11.0 mg (63% based on H_2L6' ligand).

Synthesis of BUT-104

$ZrOCl_2 \cdot 8H_2O$ (0.02 mmol, 7 mg) and H_2L7' (0.01 mmol, 4 mg) were ultrasonically dissolved in 2 mL of DMF, and formic acid (0.8 mL) was then added to the solution in a 4 mL glass vial. The vial was then heated at 120 °C for 15 days in an oven. After cooling to room temperature, the yellow block crystals of BUT-104 $[Zr_6O_4(OH)_8(L7\text{-}a)_2(H_2O)_4]$ were harvested by filtration and washed with DMF and acetone. Yield 7.5 mg (68% based on H_2L7' ligand).

Synthesis of BUT-105

$Zn(NO_3)_2 \cdot 6H_2O$ (0.02 mmol, 6 mg) and H_2L7' (0.01 mmol, 4 mg) were ultrasonically dissolved in 1 mL of DMF. To the solution in a 4 mL glass vial were added 30 μL of deionized water. The vial was sealed and then heated at 50 °C for 15 days in an oven. After cooling to room temperature, the yellow block crystals of BUT-105

[$Zn_5(OH)_2$(L7-b)$_2(H_2O)_4$] were collected by filtration, and washed with DMF and acetone. Yield 7.9 mg (82% based on H_2L7′ ligand).

Synthesis of BUT-106

$CdCl_2 \cdot 2.5H_2O$ (0.02 mmol, 5 mg) and H_2L7′ (0.01 mmol, 4 mg) were ultrasonically dissolved in 1 mL of DMF. To the solution in a 4 mL glass vial were added 0.4 mL of methanol, 0.4 mL of deionized water and 8 μL of 4 M HCl aqueous solution. The vial was sealed and then heated at 80 ^oC for 72 h in an oven. After cooling to room temperature, the lamellar crystals of BUT-107 [Cd_7(L7-c)$_4(H_2O)_{12}$] were collected by filtration, and washed with DMF and acetone. Yield 4.3 mg (47% based on H_2L7′ ligand).

Synthesis of BUT-107

$In(NO_3)_3 \cdot 6H_2O$ (0.02 mmol, 8 mg) and H_2L7′ (0.01 mmol, 4 mg) were ultrasonically dissolved in 2 mL of DMF in a 4 mL glass vial, and 16 μL of 4 M HCl aqueous solution was then added to the solution as the modulator. The vial was sealed and then heated at 100 ^oC for 48 h in an oven. After cooling down to room temperature, the yellow rhombic crystals of BUT-106 [In(L7-d)$_2$] were collected by filtration, and washed with DMF and acetone. Yield 3.3 mg (51% based on H_2L7′ ligand).

Synthesis of BUT-108

$ZrOCl_2 \cdot 8H_2O$ (0.03 mmol, 10 mg) and HL8′ (0.09 mmol, 15 mg) were ultrasonically dissolved in 2 mL of DMF, and formic acid (0.2 mL) was then added to the solution in a 4 mL glass vial. The vial was then heated at 120 ^oC for 48 h in an oven. After cooling to room temperature, the colorless block crystals of BUT-108(Zr) [$Zr_6O_4(OH)_4$(L8)$_2$(HCOO)$_6(H_2O)_2$] were harvested by filtration and washed with DMF and acetone. Yield 16 mg (57% based on HL8′ ligand).

Similar reaction with $HfCl_4$ (0.03 mmol, 10 mg) gave crystals of BUT-108(Hf) [$Hf_6O_4(OH)_4$(L8)$_2$(HCOO)$_6(H_2O)_2$]. Yield 17 mg (49% based on HL8′ ligand).

Synthesis of BUT-109

$ZrOCl_2 \cdot 8H_2O$ (0.03 mmol, 10 mg), HL9′ (0.03 mmol, 4 mg) and L9″ (0.02 mmol, 6 mg) were ultrasonically dissolved in 2 mL of DMF, and acetic acid (0.4 mL) was then added to the solution in a 4 mL glass vial. The vial was then heated at 120 °C for 24 h in an oven. After cooling to room temperature, the colorless block crystals of BUT-109(Zr) $[Zr_6O_4(OH)_{10}(L9)_3(H_2O)_6]$ were harvested by filtration and washed with DMF and acetone. Yield 6.8 mg.

Similar reaction with $HfCl_4$ (0.03 mmol, 10 mg) gave small crystals of BUT-109(Hf) $[Hf_6O_4(OH)_{10}(L9)_3(H_2O)_6]$. Yield 7.2 mg.

S4. Single crystal X-ray crystallography

The diffraction data of as-synthesized BUT-101~-109 were collected in an Agilent Supernova CCD diffractometer equipped with a mirror monochromated enhanced Cu Kα radiation (λ = 1.54184 Å). The datasets were corrected by empirical absorption correction using spherical harmonics, implemented in the SCALE3 ABSPACK scaling algorithm. The structure was solved by direct methods and refined by full-matrix least-squares on F^2 with anisotropic displacement using the SHELXTL software package. Hydrogen atoms of ligands were calculated in ideal positions with isotropic displacement parameters. Those in amino, coordinated water and hydroxyl groups were not added but were calculated into molecular formula of the crystal data. For these MOFs, the volume fractions of disordered solvents in pores could not be modeled in terms of atomic sites, but were treated by using the MASK routine in the Olex2 software package or the SQUEEZE routine in PLATON. Crystal parameters and structure refinements are summarized in Table S1~S11 (for details, see CCDC 1888829~1888839).

SXRD analyses showed that BUT-101(Cu) and BUT-101(Zn) have isostructural frameworks, consisting of the classical $M_2(COO)_4$ paddle wheel SBU (SBU = Secondary Building Units) (Fig. 1a). As expected, the H_2L6' ligand in both cases has been successfully reduced to the $L6^{2-}$ ligand in situ without the deliberate addition of

any reductant species. It is noteworthy that the newly created amino group in the $L6^{2-}$ ligand has also participated in the coordination with metals by occupying the axis sites of the paddle wheel SBUs with the angle (M−N−C) of 115.40 (BUT-101(Cu)) and 113.66° (BUT-101(Zn)), respectively. There exists a polyhedral cage in their structure, composing of six $L6^{2-}$ ligands covering the faces and six SBUs occupying the vertexes, with window size about 3.6 Å (Fig. S2a). Each cage connects fourteen adjacent cages by sharing the vertexes and faces to form the final 3D framework with 1D channels. The overall structure of BUT-101 is isoreticular with JUC-141 of the ***eea*** topology previously reported by G. Zhu et al. Due to the extended backbone of $L6^{2-}$ ligand with respect to the 5-aminoisophthlic acid, the 1D channel sizes in BUT-101 are about 6.2 Å and 12.2 Å along (111) (Fig. S2b) and (001) direction (Fig. S2c), respectively, larger than that observed in JUC-141. The solvent-accessible volume of BUT-101(Cu) and BUT-101(Zn) are estimated to be 58.3% and 56.8%, by using PLATON.

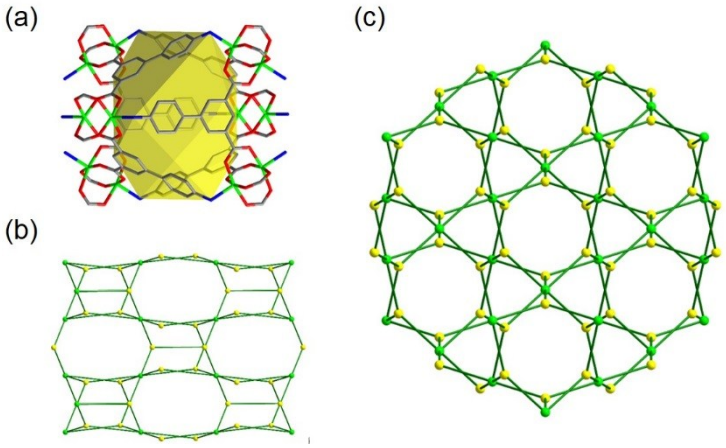

Fig. S2 (a) The polyhedral cage in BUT-101 and the topological representation of BUT-101 network with 1D channels along the (b) (111) and (c) (001) direction, respectively.

BUT-102 crystallizes in the triclinic crystal system with the $P\bar{1}$ space group. The asymmetric unit contains one Cd(II) ion, one $L6^{2-}$ ligand, and a water molecule. The 6-coordinated Cd(II) center adopts a distorted quadrangular bipyramid coordination geometry, which are generated by four O atoms from three carboxylates, one N atom of the amino on the $L6^{2-}$ ligand, and one from the terminal water molecule. Among

the coordinated carboxylates, one is chelated to the Cd(II) ion, and another two carboxylate groups bridge two adjacent Cd(II) ions by the bimonodentate coordination. Two identical Cd(II) centers are linked into a Cd_2 SBU by two bridging carboxylates from two different $L6^{2-}$ ligands (Fig. S3). Each Cd_2 SBU connects to four $L6^{2-}$ ligands, and each ligand connects to three Cd_2 SBUs to form a 2D layer (Fig. 1b). These layers stack through H-bond and π-π interactions of adjacent parallel benzene rings (distance of benzene centers of about 6.1 Å) to form the final 3D structure of BUT-102.

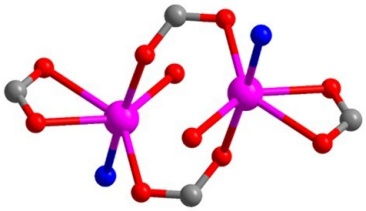

Fig. S3 The Cd_2 cluster in BUT-102.

BUT-103 crystallizes in the monoclinic crystal system (space group $P2_1$). There are two six-coordinated Mn ions, two $L6^{2-}$ ligands, three DMF coordinated molecules and two free DMF molecules in the asymmetric unit. Mn1 is connected with four carboxylate groups from four different $L6^{2-}$ ligands, among which one is chelated to Mn1 atom, two are bimonodentate carboxylates, and another adopts the (μ^2-η^2:η^1) coordination mode. Mn2 adopts a distorted octahedral coordination geometry through linking to three carboxylate groups from three different $L6^{2-}$ ligands, including two bimonodentate carboxylate groups shared with Mn1 and the (μ^2-η^2:η^1) carboxylate, as well as three DMF molecules occupying another three vertexes of the octahedron. Mn1 and Mn2 are bridged into a Mn_2 cluster by three carboxylates (Fig. S4). Each Mn_2 SBU connects to four carboxyl groups from four different $L6^{2-}$ ligands, and each ligand connects to two Mn_2 SBUs with the free amino groups extending outward, affording a 2D layer (Fig. 1c). These 2D layers stack through H-bond interactions to form the 3D structure of BUT-103.

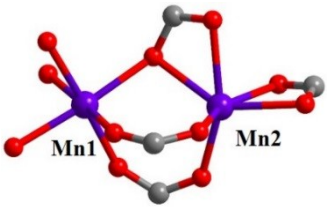

Fig. S4 The Mn_2 cluster in BUT-103.

BUT-104 crystallizes in the monoclinic crystal system (β = 92.956(7)°, space group *C*2/m). In BUT-104, the diazo-bond-coupled tetra-topic carboxylate ligand L7-a^{4-} can be viewed as a planar rhomboid 4-connected linker and the typical Zr_6O_8 cluster serves as an 8-connected node, and the entire framework is similar to those of NU-901, NU-902 and NPF-300 with the rare ***scu*** topology (Fig. 2a and S5). Large 1D rhombic channels (the diagonal distances of the pores are about 9.6 and 23.8 Å) could be observed in the framework along the *c*-axis of crystallography. The total solvent-accessible volume in the framework of BUT-104 is estimated to be 75.3%, by using PLATON.

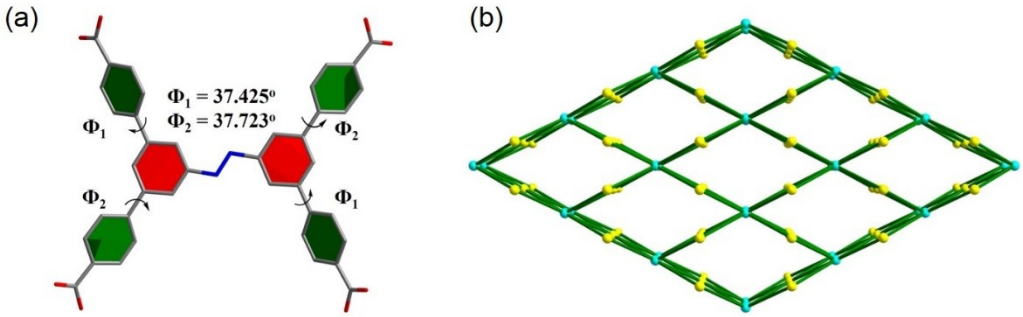

Fig. S5 (a) The dihedral angles of ligand L7-a^{4-} in BUT-104 network and (b) the topological representation of BUT-104 network with 1D channels along the *c*-axis.

BUT-105 crystallizes in the trigonal crystal system (space group *Rc*). There is two and a half crystallographically independent Zn atoms in the asymmetric unit. The six-coordinated Zn1 atom is linked with four oxygen atoms from four different bimonodentate carboxylates of four L7-b^{4-} ligands and two μ3-O atoms. The four-coordinated Zn2 atom is connected with three carboxylate oxygen atoms from three different carboxylates of three L7-b^{4-} ligands and one μ3-O atom. The five-coordinated Zn3 atom connects to two oxygen atoms from two different

bimonodentate carboxylates of two L7-b ligands, one μ3-O atom, and two oxygen atoms from two terminal water molecules. Two Zn1 atoms, two Zn3 atoms and one Zn2 atom are bridged by two μ3-O atoms to form a Zn_5 cluster (Fig. S6a). Each such Zn_5 building unit connects to eight carboxylates, among which two are monodentate carboxylate, and the others are bimonodentate carboxylates. These carboxylates are from eight different L7-b^{4-} ligands stretching toward four orientations with two ligands stacking staggered in the same direction through π-π interactions of parallel benzene rings. It is worth noting that different with the rhomboid azoic ligand of BUT-104, the L7-b^{4-} ligand of BUT-105 was generated in an oxidation form of the diazo bond, which could be viewed as an approximate planar rectangular linker. However, the dihedral angles between the central plane and four peripheral benzene rings are different to match the linkage geometry of Zn_5 clusters (Fig. S6b). Each L7-b^{4-} ligand links to four Zn_5 clusters to give a final 3D framework with nano-sized hexagonal channels in diameter of about 4.0 nm along the *c*-axis. Topologically, the Zn_5 SBU can be regarded as an eight-connected node and the L7-b^{4-} ligand can act as a four-connected linker. Thus the resulting 3D framework can be simplified as a (4,8)-connected network with the point symbol of $(4^{12}.6^{16})(4^6)_2$, which has not been reported in the literature yet (Fig. S6c). The solvent accessible volume of BUT-105 is up to 76.3% of the total volume, as estimated by PLATON.

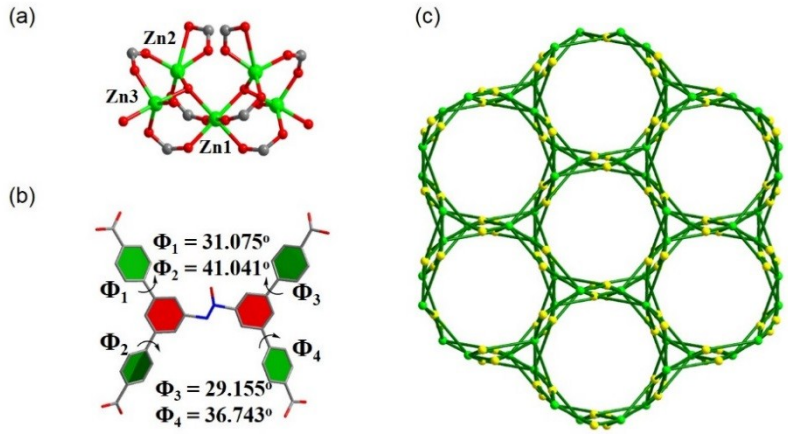

Fig. S6 (a) The Zn_5 cluster and (b) azoxy ligand L7-b^{4-} with different dihedral angles in BUT-105, and (c) the topological representation of BUT-105 network with 1D channels along the *c*-axis.

BUT-106 crystallizes in the monoclinic space group *C*2/*c*. The asymmetric unit contains four crystallographically independent Cd(II) ions. The single Cd1 connects four monodentate carboxylates from four different L7-c^{4-} ligands (Fig. S7a and 2c). Six-coordinated Cd2, seven-coordinated Cd3 and four-coordinated Cd4 are bridged by six carboxylate groups from six different L7-c^{4-} ligands to form a trimeric Cd_3 SBU, and five H_2O complete remaining coordination (Fig. S7b). Among the six carboxylates, two monodentate ones are linking to Cd4, and the rest adopt the (μ^2-η^2:η^1) coordination when linking to Cd2 and Cd3. Similar to that in BUT-105, the L7-c^{4-} ligand in BUT-106 was also generated with an oxidized diazo bond. However, the azoxy L7-c^{4-} displays two different configurations, which is resulted from varying dihedral angles between the central plane and four peripheral benzene rings in different coordination (Fig. S7c and d). These L7-c^{4-} ligands connect to single Cd(II) ion and Cd_3 SBU alternately, forming the complex (4,4,4,6)-connected 3D framework with the new topology [point symbol of $(4^2.8^4)(4^3.6^2.8)_4(4^9.6^6)_2$] (Fig. S7e). In the final 3D structure, π-π interactions of adjacent parallel benzene rings could be observed between these stacking L7-c^{4-} ligands when binding to Cd(II) centers. The solvent accessible volume of BUT-106 is 37.6% of the total volume, as estimated by PLATON.

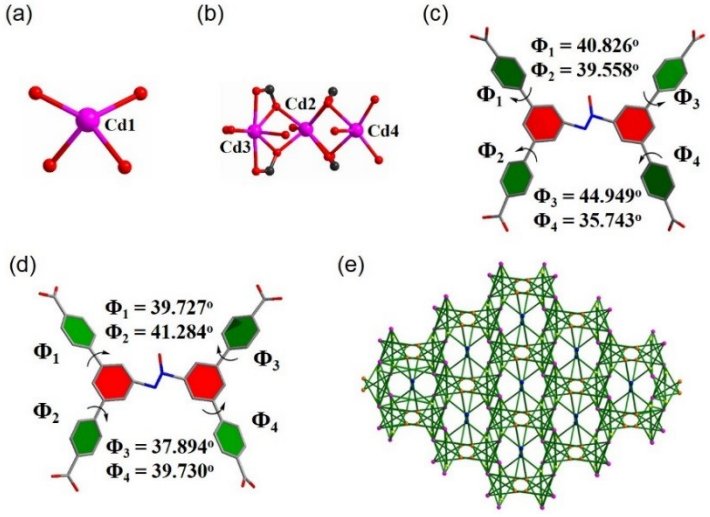

Fig. S7 (a) The single Cd(II) node, (b) Cd_3 cluster, (c), (d) two configurations of azoxy ligand L7-c^{4-} with different dihedral angles in BUT-106, and (e) the topological representation of BUT-106 network along the *c*-axis.

BUT-107 crystallizes in the orthorhombic crystal system with *Pnna* space group. The asymmetric unit contains one single In(III) ion and one L7-d^{4-} ligand (Fig. S8a and 2d). The In(III) center adopts a distorted square-antiprismatic coordination geometry by bridging four carboxylates from four different L7-d^{4-} ligands. All the carboxylates on the L7-d ligand chelate to the In(III) ion, and each L7-d^{4-} ligand connects to four In(III) ions to form a single 3D anionic network with 1D channels along *b*- and *c*- axis, respectively. Due to the large void in the framework, two such identical and independent single frameworks mutually interpenetrate, reinforcing each other via intermolecular π-π interaction between the adjacent parallel benzene rings. Interestingly, for the *trans*-azoic ligand L7-d^{4-} in BUT-107, two terphenyl moieties on two sides of the central diazo bond display a spatial configuration and the dihedral angle between two central benzene rings is 83.281°, close to the right-angle (Fig. S8b). Topologically, the spatial 4-connected L7-d^{4-} linker and 4-connected In(III) node connect alternately to give the single 3D framework with the ***ion*** topology (Fig. S8c and S8d). The solvent accessible volume of the two-fold interpenetrated BUT-107 is 72.0% of the total volume, as estimated by PLATON.

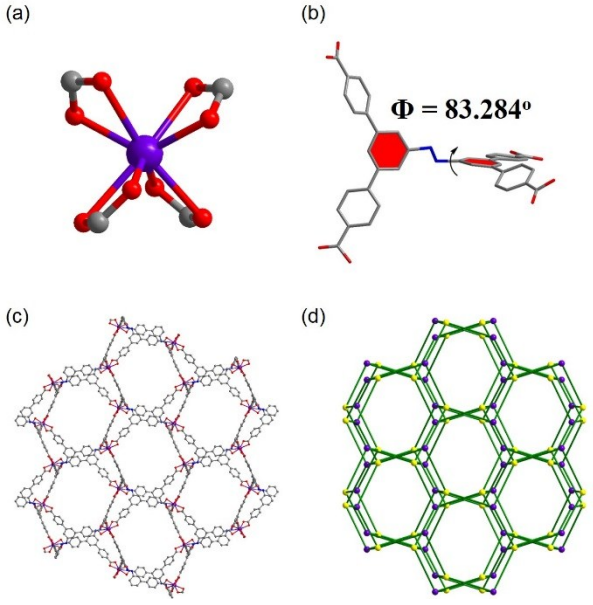

Fig. S8 (a) The single In(III) ion and (b) the L7-d^{4-} ligand with two terphenyl moieties nearly perpendicular in BUT-107. (c) The single anionic framework, and (d) the topological representation of BUT-107 viewed along the *c*-axis.

BUT-108(Zr) and BUT-108(Hf) are isostructural (Fig. 3). A two-fold interpenetration could be observed in their structure, and the single framework is isostructural with PCN-777 (***spn*** topology) stacked by two kinds of cages, causing the face of tetrahedral cage in PCN-777 to extrude. In PCN-777, the TATB organic ligand displays a trigonal-planar geometry, while for BUT-108, the ligand $L8^{3-}$ is in a flat tripod shape (Fig. S9). In BUT-108, six terminal $HCOO^-$ (two are in monodentate coordination) and two H_2O entries complete the remaining coordination of the cluster and account for the charge balance. Owning to the interpenetration of frameworks, the solvent accessible volume in BUT-108(Zr) and BUT-108(Hf) are just 64.1% of the total volume, much less than that in PCN-777, as estimated by PLATON.

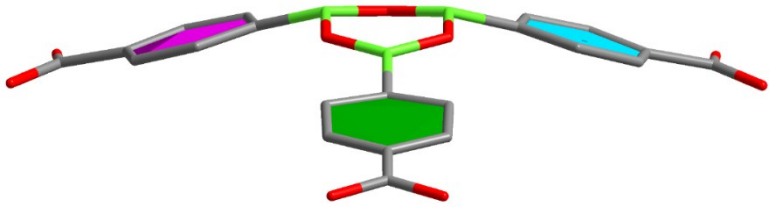

Fig. S9 The tripod-shaped ligand $L8^{3-}$ in BUT-108.

BUT-109(Zr) has a 3D framework structure constructed from Zr_6 clusters and $L9^{2-}$ ligands, seemingly adopting a ***ftw*** topology with two-fold interpenetration (Fig. 4). Due to the crystallographically imposed symmetry, the $L9^{2-}$ ligand in the structure model is in disorder (Fig. S10). The structural refinement of BUT-109(Zr) indicates that the occupancy of $L9^{2-}$ ligands is close to 0.5. The linear di-carboxylate $L9^{2-}$ ligand was produced from the in situ condensation of HL9′ and L9″, acting as a 2-connected linker actually. Statistically, the Zr_6 clusters are linked by six $L9^{2-}$ ligands to form the final 3D framework. Missing linkers thus lead to defects in this *pseudo* 4,12-connected framework and OH/OH_2 entities complete the remaining coordination of the $Zr_6O_4(OH)_4$ cluster. Overall, BUT-109(Zr) might have a 6-connected network with full occupancy of $L9^{2-}$ ligand, or other cases, and the formula could be $[Zr_6O_4(OH)_{10}(L9)_3(H_2O)_6]$.

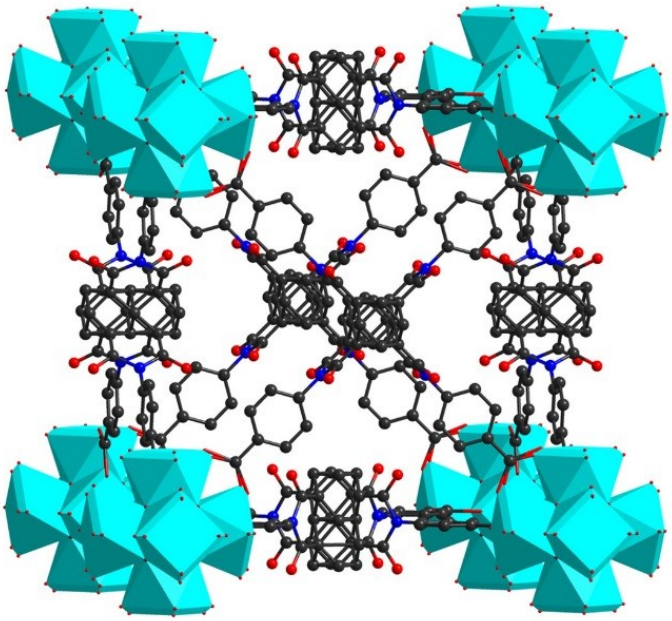

Fig. S10 The *pseudo* 4,12-connected single framework of BUT-109(Zr) with $L9^{2-}$ ligand in disorder.

Table S1. The crystallographic data and structure refinement for BUT-101(Cu).

Formula	$CuC_{14}H_{13}O_6N$
M	354.80
Crystal system	Trigonal
Space goup	$R\bar{3}m$
a / Å	18.6355(7)
b / Å	18.6355(7)
c / Å	34.4019(12)
α / °	90
β / °	90
γ / °	120
V / Å^3	10346.5(9)
Z	18
D_C / g cm^{-3}	0.921
μ / mm^{-1}	1.413
T / K	173.01(10)
Reflections collected	7625
Independent reflections	2276 [R_{int} = 0.0302, R_{sigma} = 0.0257]
Goodness-of-fit on F^2	1.086
R_1[a], wR_2[b] [$I > 2\sigma(I)$]	R_1 = 0.0381, wR_2 = 0.1216
R_1[a], wR_2[b] (all data)	R_1 = 0.0408, wR_2 = 0.1244
Largest diff. peak and hole (e.Å^{-3})	0.35 / -0.64

[a] $R_1=\Sigma||F_o|-|F_c|| / \Sigma|F_o|$

[b] $wR_2=\{\Sigma[w(F_o^2-F_c^2)^2] / [w(F_o^2)^2]\}^{1/2}$, $[F_o > 4\sigma(F_o)]$

Table S2. The crystallographic data and structure refinement for BUT-101(Zn).

Formula	$ZnC_{14}H_{13}O_6N$
M	356.64
Crystal system	Trigonal
Space goup	$R\bar{3}m$
a / Å	18.4038(8)
b / Å	18.4038(8)
c / Å	34.5026(19)
α / °	90
β / °	90
γ / °	120
V / Å^3	10120.4(10)
Z	18
D_C / g cm^{-3}	0.947
μ / mm^{-1}	1.591
T / K	150.00(10)
Reflections collected	7259
Independent reflections	2221 [R_{int} = 0.0595, R_{sigma} = 0.0446]
Goodness-of-fit on F^2	1.088
R_1[a], wR_2[b] [$I > 2\sigma(I)$]	R_1 = 0.0602, wR_2 = 0.1639
R_1[a], wR_2[b] (all data)	R_1 = 0.0645, wR_2 = 0.1673
Largest diff. peak and hole (e.Å^{-3})	1.28 / -0.55

[a] $R_1=\Sigma||F_o|-|F_c|| / \Sigma|F_o|$

[b] $wR_2=\{\Sigma[w(F_o^2-F_c^2)^2] / [w(F_o^2)^2]\}^{1/2}$, $[F_o>4\sigma(F_o)]$

Table S3. The crystallographic data and structure refinement for BUT-102.

Formula	$CdC_{14}H_{11}O_5N$
M	385.64
Crystal system	Triclinic
Space goup	$P\bar{1}$
a / Å	7.6897(3)
b / Å	8.7992(3)
c / Å	12.7198(4)
α / °	87.203(3)
β / °	74.302(3)
γ / °	76.159(3)
V / Å^3	804.39(5)
Z	2
D_C / g cm^{-3}	1.592
μ / mm^{-1}	11.054
T / K	292.50(4)
Reflections collected	8628
Independent reflections	2871[R_{int} = 0.0397, R_{sigma} = 0.0387]
Goodness-of-fit on F^2	1.046
R_1[a], wR_2[b] [$I > 2\sigma(I)$]	R_1 = 0.0327, wR_2 = 0.0836
R_1[a], wR_2[b] (all data)	R_1 = 0.0356, wR_2 = 0.0860
Largest diff. peak and hole (e.Å^{-3})	0.81 / -0.67

[a] $R_1=\Sigma||F_o|-|F_c|| / \Sigma|F_o|$

[b] $wR_2=\{\Sigma[w(F_o^2-F_c^2)^2] / [w(F_o^2)^2]\}^{1/2}$, $[F_o>4\sigma(F_o)]$

Table S4. The crystallographic data and structure refinement for BUT-103.

Formula	$Mn_4C_{74}H_{78}O_{22}N_{10}$
M	1679.24
Crystal system	Monoclinic
Space goup	$P2_1$
a / Å	10.0867(10)
b / Å	15.6900(2)
c / Å	15.2941(2)
α / °	90
β / °	105.4640(10)
γ / °	90
V / Å^3	2332.82(5)
Z	1
D_C / g cm^{-3}	1.351
μ / mm^{-1}	4.963
T / K	293.00(2)
Reflections collected	40263
Independent reflections	7367 [R_{int} = 0.0302, R_{sigma} = 0.0214]
Goodness-of-fit on F^2	1.074
R_1[a], wR_2[b] [$I > 2\sigma(I)$]	R_1 = 0.0463, wR_2 = 0.1304
R_1[a], wR_2[b] (all data)	R_1 = 0.0472, wR_2 = 0.1312
Largest diff. peak and hole (e.Å^{-3})	0.99 / -0.49

[a] $R_1=\Sigma||F_o|-|F_c|| / \Sigma|F_o|$

[b] $wR_2=\{\Sigma[w(F_o^2-F_c^2)^2] / [w(F_o^2)^2]\}^{1/2}$, $[F_o>4\sigma(F_o)]$

Table S5. The crystallographic data and structure refinement for BUT-104.

Formula	$Zr_3C_{40}H_{26}O_{18}N_2$
M	1096.25
Crystal system	Monoclinic
Space goup	*C2/m*
a / Å	35.346(2)
b / Å	18.477(4)
c / Å	18.0998(12)
α / °	90
β / °	92.956(7)
γ / °	90
V / Å^3	11805(3)
Z	4
D_C / g cm^{-3}	0.597
μ / mm^{-1}	2.362
T / K	173.00(10)
Reflections collected	22058
Independent reflections	9846 [R_{int} = 0.1807, R_{sigma} = 0.2013]
Goodness-of-fit on F^2	0.927
R_1[a], wR_2[b] [$I > 2\sigma(I)$]	R_1 = 0.1305, wR_2 = 0.3114
R_1[a], wR_2[b] (all data)	R_1 = 0.1846, wR_2 = 0.3681
Largest diff. peak and hole (e.Å^{-3})	3.51 / -1.58

[a] $R_1=\Sigma||F_o|-|F_c|| / \Sigma|F_o|$

[b] $wR_2=\{\Sigma[w(F_o^2-F_c^2)^2] / [w(F_o^2)^2]\}^{1/2}$, $[F_o>4\sigma(F_o)]$

Table S6. The crystallographic data and structure refinement for BUT-105.

Formula	$Zn_5C_{80}H_{54}O_{27}N_4$
M	1830.26
Crystal system	Trigonal
Space goup	$R\bar{3}c$
a / Å	54.3601(10)
b / Å	54.3601(10)
c / Å	42.0659(13)
α / °	90
β / °	90
γ / °	120
V / Å^3	107652(5)
Z	18
D_C / g cm^{-3}	0.492
μ / mm^{-1}	0.780
T / K	173.01(10)
Reflections collected	116821
Independent reflections	20392 [R_{int} = 0.1084, R_{sigma} = 0.0651]
Goodness-of-fit on F^2	1.001
R_1[a], wR_2[b] [$I > 2\sigma(I)$]	R_1 = 0.0938, wR_2 = 0.2655
R_1[a], wR_2[b] (all data)	R_1 = 0.1460, wR_2 = 0.3082
Largest diff. peak and hole (e.Å^{-3})	0.35 / -0.40

[a] $R_1=\Sigma||F_o|-|F_c|| / \Sigma|F_o|$

[b] $wR_2=\{\Sigma[w(F_o^2-F_c^2)^2] / [w(F_o^2)^2]\}^{1/2}$, $[F_o>4\sigma(F_o)]$

Table S7. The crystallographic data and structure refinement for BUT-106.

Formula	$Cd_7C_{160}H_{112}O_{48}N_8$
M	3701.54
Crystal system	Monoclinic
Space goup	*C*2/*c*
a / Å	32.872(2)
b / Å	19.2171(7)
c / Å	32.400(3)
α / °	90
β / °	105.239(9)
γ / °	90
V / Å^3	19748(3)
Z	4
D_C / g cm^{-3}	1.240
μ / mm^{-1}	6.500
T / K	173.00(10)
Reflections collected	36069
Independent reflections	17166 [R_{int} = 0.0667, R_{sigma} = 0.0931]
Goodness-of-fit on F^2	0.909
R_1[a], wR_2[b] [$I > 2\sigma(I)$]	R_1 = 0.1068, wR_2 = 0.2963
R_1[a], wR_2[b] (all data)	R_1 = 0.1747, wR_2 = 0.3422
Largest diff. peak and hole (e.Å^{-3})	1.91 / -0.80

[a] $R_1=\Sigma||F_o|-|F_c|| / \Sigma|F_o|$

[b] $wR_2=\{\Sigma[w(F_o^2-F_c^2)^2] / [w(F_o^2)^2]\}^{1/2}$, $[F_o>4\sigma(F_o)]$

Table S8. The crystallographic data and structure refinement for BUT-107.

Formula	$InC_{80}H_{44}O_8N_2$
M	1276.06
Crystal system	Orthorhombic
Space goup	*Pnna*
a / Å	32.0315(3)
b / Å	28.2049(3)
c / Å	19.8600(2)
α / °	90
β / °	90
γ / °	90
V / Å^3	17942.4(3)
Z	8
D_C / g cm^{-3}	0.573
μ / mm^{-1}	2.291
T / K	243.00(2)
Reflections collected	79338
Independent reflections	15832 [R_{int} = 0.0422, R_{sigma} = 0.0361]
Goodness-of-fit on F^2	1.031
R_1[a], wR_2[b] [$I > 2\sigma(I)$]	R_1 = 0.0706, wR_2 = 0.2197
R_1[a], wR_2[b] (all data)	R_1 = 0.0804, wR_2 = 0.2308
Largest diff. peak and hole (e.Å^{-3})	0.62 / -0.42

[a] $R_1=\Sigma||F_o|-|F_c|| / \Sigma|F_o|$

[b] $wR_2=\{\Sigma[w(F_o^2-F_c^2)^2] / [w(F_o^2)^2]\}^{1/2}$, $[F_o>4\sigma(F_o)]$

Table S9. The crystallographic data and structure refinement for BUT-108(Zr).

Formula	$Zr_3C_{24}H_{19}O_{20}B_3$
M	933.50
Crystal system	Tetragonal
Space goup	$I4_1/amd$
a / Å	40.5746(8)
b / Å	40.5746(8)
c / Å	17.0198(4)
α / °	90
β / °	90
γ / °	90
V / Å^3	28019.7(13)
Z	16
D_C / g cm^{-3}	0.879
μ / mm^{-1}	3.956
T / K	173.00(10)
Reflections collected	26464
Independent reflections	6381 [R_{int} = 0.0861, R_{sigma} = 0.0625]
Goodness-of-fit on F^2	1.158
R_1[a], wR_2[b] [$I > 2\sigma(I)$]	R_1 = 0.1028, wR_2 = 0.2872
R_1[a], wR_2[b] (all data)	R_1 = 0.1378, wR_2 = 0.3466
Largest diff. peak and hole (e.Å^{-3})	1.15 / -2.40

[a] $R_1=\Sigma||F_o|-|F_c|| / \Sigma|F_o|$

[b] $wR_2=\{\Sigma[w(F_o^2-F_c^2)^2] / [w(F_o^2)^2]\}^{1/2}$, $[F_o>4\sigma(F_o)]$

Table S10. The crystallographic data and structure refinement for BUT-108(Hf).

Formula	$Hf_3C_{24}H_{19}O_{20}B_3$
M	1195.30
Crystal system	Tetragonal
Space goup	$I4_1/amd$
a / Å	40.4997(4)
b / Å	40.4997(4)
c / Å	16.9534(4)
α / °	90
β / °	90
γ / °	90
V / Å^3	27807.4(9)
Z	16
D_C / g cm^{-3}	1.136
μ / mm^{-1}	8.422
T / K	293.00(2)
Reflections collected	42600
Independent reflections	6304 [R_{int} = 0.0542, R_{sigma} = 0.0344]
Goodness-of-fit on F^2	1.074
R_1[a], wR_2[b] [$I > 2\sigma(I)$]	R_1 = 0.0593, wR_2 = 0.1742
R_1[a], wR_2[b] (all data)	R_1 = 0.0673, wR_2 = 0.1842
Largest diff. peak and hole (e.Å^{-3})	0.83 / -1.55

[a] $R_1=\Sigma||F_o|-|F_c|| / \Sigma|F_o|$

[b] $wR_2=\{\Sigma[w(F_o^2-F_c^2)^2] / [w(F_o^2)^2]\}^{1/2}$, $[F_o>4\sigma(F_o)]$

Table S11. The crystallographic data and structure refinement for BUT-109(Zr).

Formula	$Zr_6C_{84}H_{58}O_{44}N_6$
M	2402.73
Crystal system	Cubic
Space goup	$Im\bar{3}m$
a / Å	19.225(2)
b / Å	19.225(2)
c / Å	19.225(2)
α / °	90
β / °	90
γ / °	90
V / Å^3	7105(2)
Z	2
D_C / g cm^{-3}	1.107
μ / mm^{-1}	4.047
T / K	173.01(10)
Reflections collected	2875
Independent reflections	601 [R_{int} = 0.0958, R_{sigma} = 0.0488]
Goodness-of-fit on F^2	0.968
R_1[a], wR_2[b] [$I > 2\sigma(I)$]	R_1 = 0.1105, wR_2 = 0.2898
R_1[a], wR_2[b] (all data)	R_1 = 0.1510, wR_2 = 0.3488
Largest diff. peak and hole (e.Å^{-3})	0.91 / -0.64

[a] $R_1=\Sigma||F_o|-|F_c|| / \Sigma|F_o|$

[b] $wR_2=\{\Sigma[w(F_o^2-F_c^2)^2] / [w(F_o^2)^2]\}^{1/2}$, $[F_o>4\sigma(F_o)]$

S5. Powder X-ray diffraction

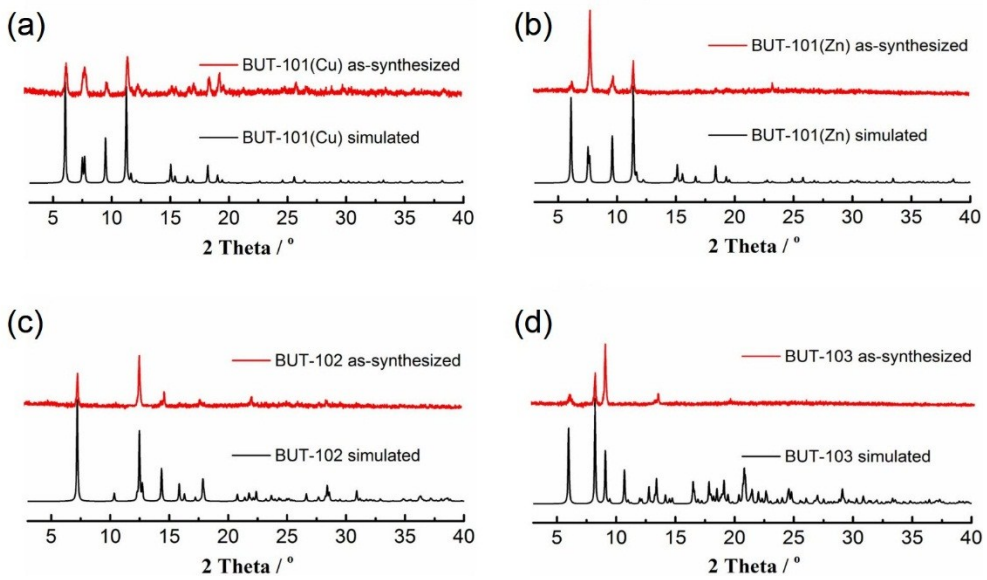

Fig. S11 PXRD patterns for (a) BUT-101(Cu), (b) BUT-101(Zn), (c) BUT-102, and (d) BUT-103.

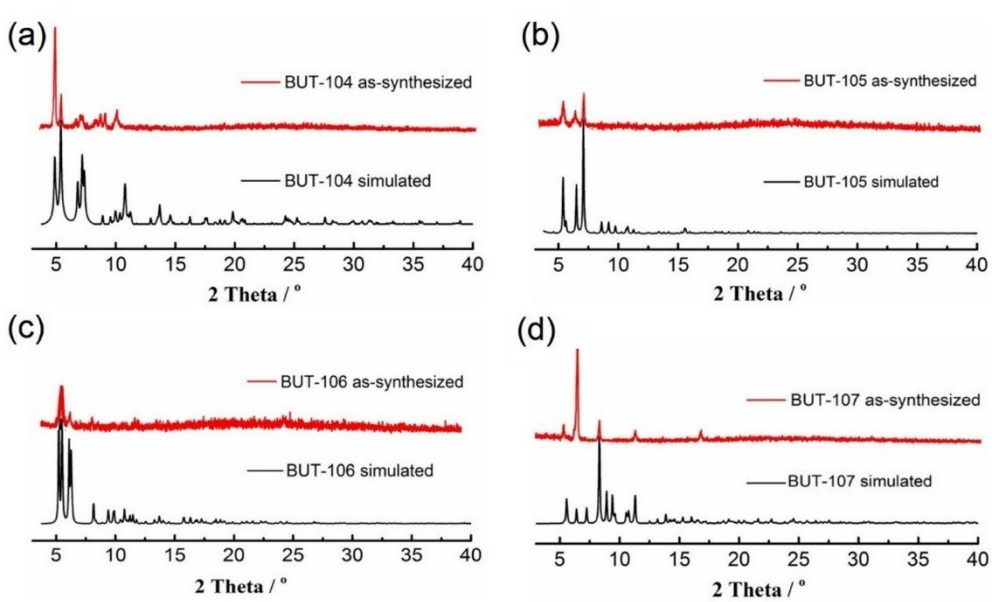

Fig. S12 PXRD patterns for (a) BUT-104, (b) BUT-105, (c) BUT-106, and (d) BUT-107.

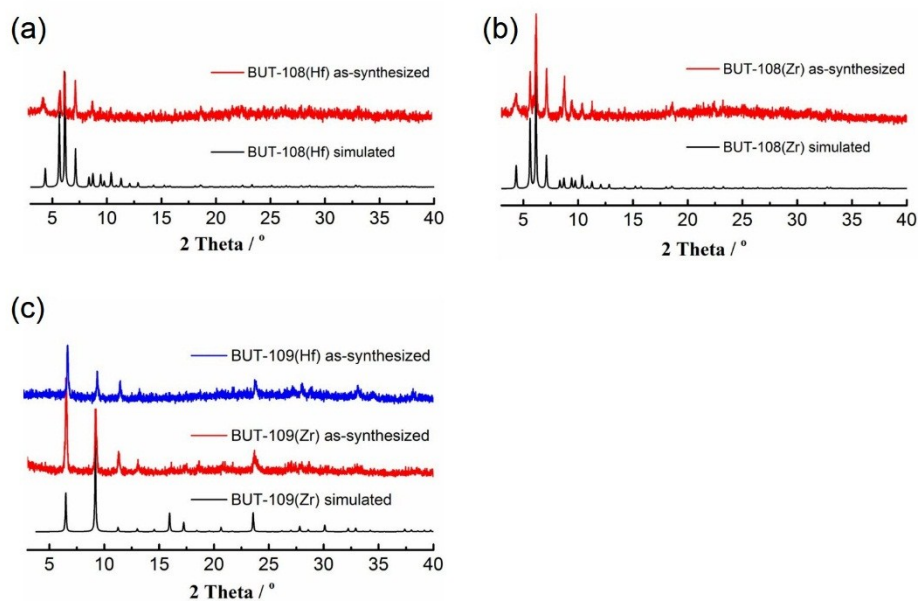

Fig. S13 PXRD patterns for (a) BUT-108(Zr), (b) BUT-108(Hf) and (d) BUT-109.

S6. Activation of the MOF samples

Before NMR, N_2 adsorption, FT-IR and TGA measurements, a suspension of as-synthesized sample (about 80 mg for each sample of BUT-101~-109) in 10 mL fresh DMF was placed in a centrifuge tube and heated at 80 °C for 24 h in a conventional oven. The sample was soaked in acetone (10 mL) for 2 days at room temperature, when fresh solvents were exchanged every 12 h. The sample was collected by decanting and dried in air. Before tests, the dry sample was loaded in a sample tube and further activated under high vacuum at the temperature of 60 °C for 5 h.

S7. FT-IR

FT-IR spectra of samples for BUT-101~-109 were recorded in comparison with the precursors, respectively, to test the coordination between newly formed ligands to metal species in the solvo-thermal reaction, as shown in Fig. S14~S17.

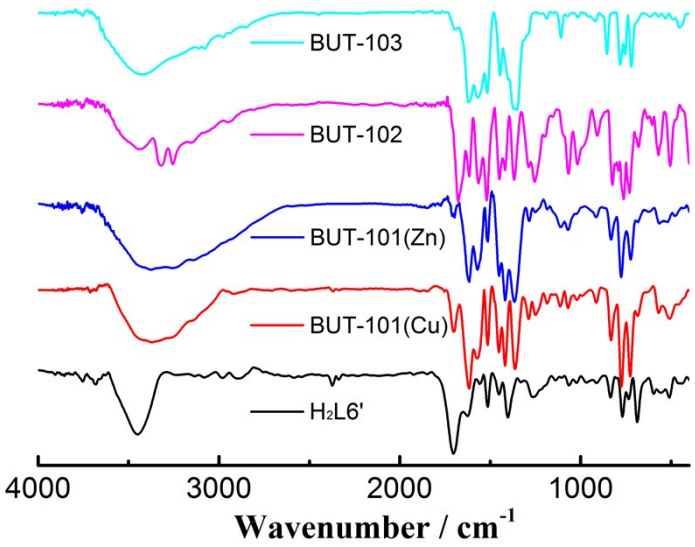

Fig. S14 FT-IR spectra of H_2L6' and BUT-101~-103.

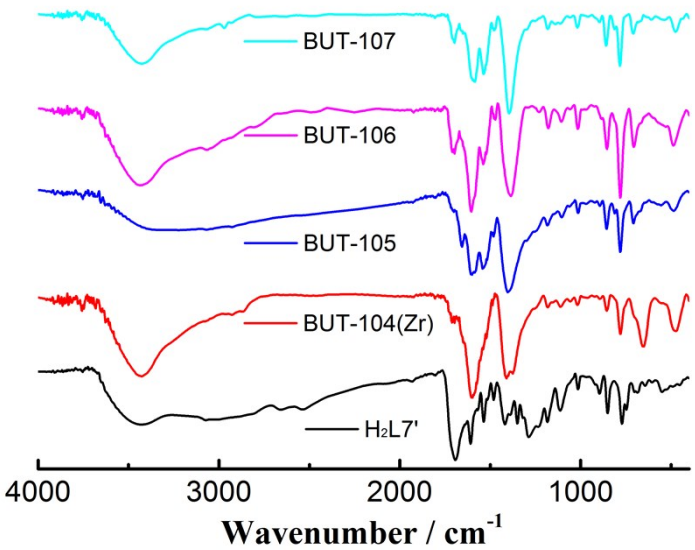

Fig. S15 FT-IR spectra of H_2L7' and BUT-104~-107.

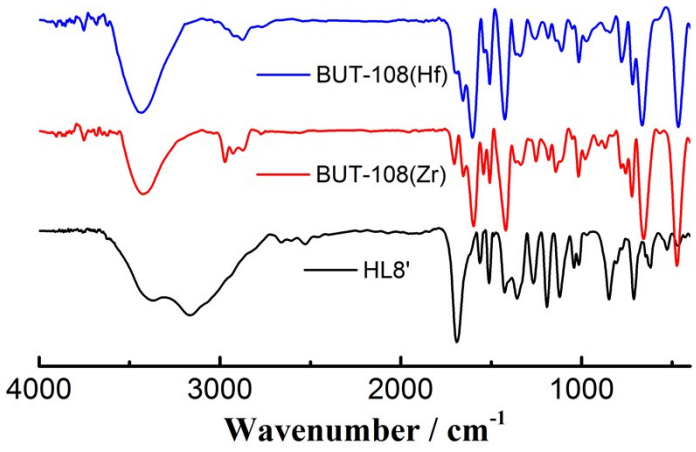

Fig. S16 FT-IR spectra of HL8′ and BUT-108.

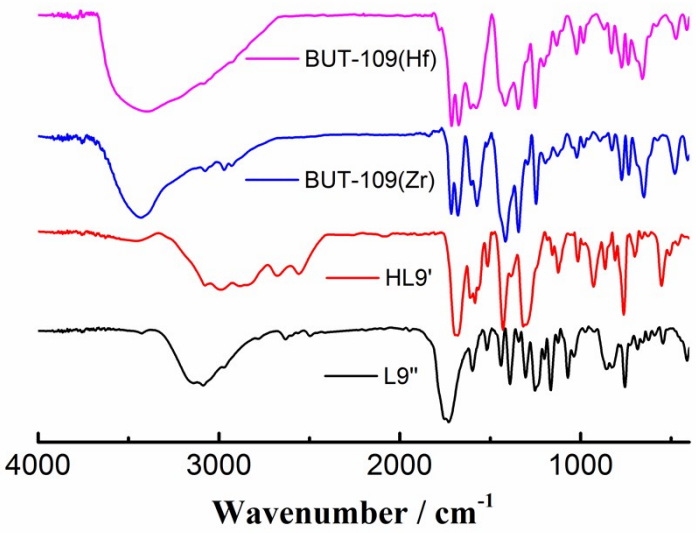

Fig. S17 FT-IR spectra of HL9′, L9″ and BUT-109.

S8. TGA

To evaluate the thermal stability of BUT-101~-109, TGA measurements of their samples were conducted and resulted curves are shown in Fig. S18.

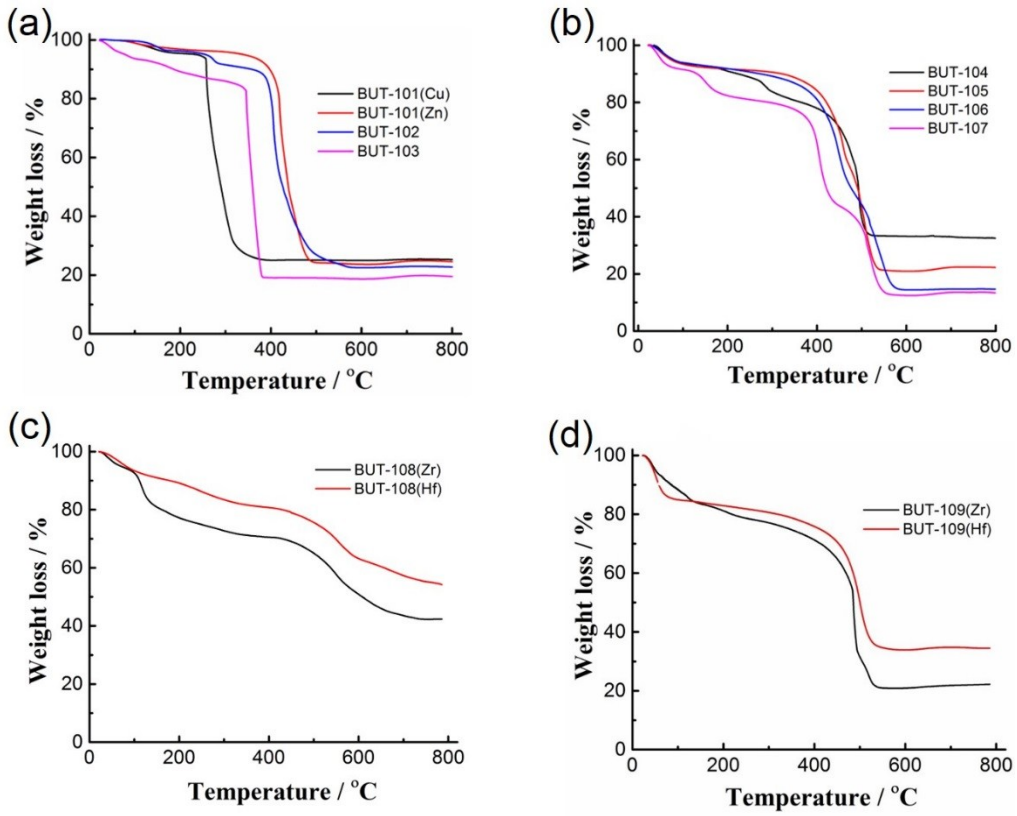

Fig. S18 TGA curves of (a) BUT-101~103, (b) BUT-104~107, (c) BUT-108 and (d) BUT-109.

S9. Elemental Analysis

After activation and evacuation of BUT-101–109 samples, their elemental analyses were measured.

BUT-101(Cu): Anal. Calc. for $CuC_{14}H_{13}NO_6$ C, 47.39; H, 3.69; N, 3.95; found C, 47.31; H, 3.78; N, 3.89.

BUT-101(Zn): Anal. Calc. for $ZnC_{14}H_{13}NO_6$ C, 47.15; H, 3.67; N, 3.93; found C, 47.11; H, 3.76; N, 3.90.

BUT-102: Anal. Calc. for $CdC_{14}H_{11}NO_5$ C, 43.60; H, 2.88; N, 3.63; found C, 43.65; H, 2.94; N, 3.57.

BUT-103: Anal. Calc. for $Mn_4C_{74}H_{78}N_{10}O_{22}$ C, 52.93; H, 4.68; N, 8.34; found C, 52.88; H, 4.80; N, 8.38.

BUT-104: Anal. Calc. for $Zr_3C_{40}H_{26}N_2O_{18}$ C, 43.82; H, 2.39; N, 2.56; found C, 43.87; H, 2.51; N, 2.49.

BUT-105: Anal. Calc. for $Zn_5C_{80}H_{54}N_4O_{27}$ C, 52.50; H, 2.97; N, 3.06; found C, 52.41; H, 3.07; N, 3.02.

BUT-106: Anal. Calc. for $Cd_7C_{160}H_{112}N_8O_{48}$ C, 51.92; H, 3.05; N, 3.03; found C, 51.89; H, 3.23; N, 2.95.

BUT-107: Anal. Calc. for $InC_{80}H_{44}N_2O_8$ C, 75.30; H, 3.48; N, 2.20; found C, 75.43; H, 3.57; N, 2.16.

BUT-108(Zr): Anal. Calc. for $Zr_3C_{24}H_{19}B_3O_{20}$ C, 30.88; H, 2.05; found C, 30.79; H, 2.27.

BUT-108(Hf): Anal. Calc. for $Hf_3C_{24}H_{19}B_3O_{20}$ C, 24.12; H, 1.60; found C, 24.03; H, 1.83.

BUT-109(Zr): Anal. Calc. for $Zr_6C_{84}H_{58}N_6O_{44}$ C, 41.99; H, 2.43; N, 3.50; found C, 42.07; H, 2.84; N, 3.41.

BUT-109(Hf): Anal. Calc. for $Hf_6C_{84}H_{58}N_6O_{44}$ C, 34.48; H, 2.00; N, 2.87; found C, 34.33; H, 2.35; N, 2.71.

S10. ^{1}H NMR Test

The ^{1}H NMR spectra of H_2L6′, H_2L7′ and HL8′ precursors are shown in Fig. S19, S21 and S24. Before NMR test, the activated samples of BUT-101(Zn) and -108(Zr) (about 20 mg for each) were immersed into a mixture of six drops of DCl (37%) and 0.5 mL of DMSO-d_6, and ultrasonically dissolved, respectively. The samples of BUT-104–-107 were similarly treated with D_2SO_4 (98%)/DMSO-d_6. Then the uniform samples were used for ^{1}H NMR test. From the spectra it was found that L7-a and -d (in BUT-104 and -107) as well as L7-b and -c (in BUT-105 and 106) have similar NMR peaks, indicating their same identity. Therefore, spectra of L7-a and -b were taken as the example, respectively. The recorded spectra of L6 (in BUT-101(Zn)), L7-a (in BUT-104), L7-b (in BUT-105), and acidized L8 (in BUT-108(Zr)) are as represented in Fig. S20, S22, S23 and S25. Regrettably, massive efforts on dissolving samples of BUT-109(Zr) and -109(Hf) with various reagents and solvents have failed due to the extremely poor solubility of bulky L9 ligand.

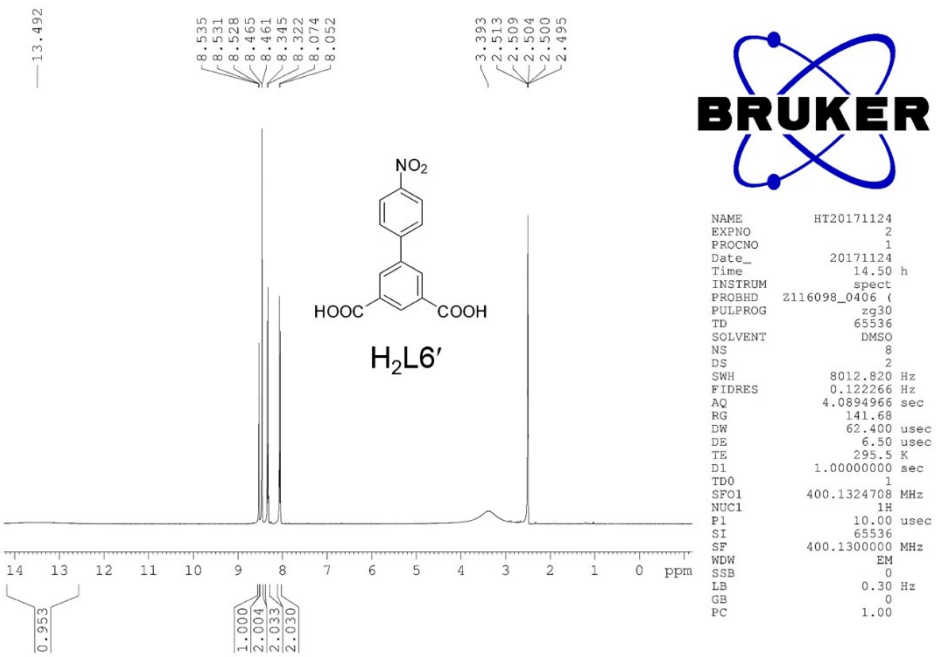

Fig. S19 ^{1}H NMR spectrum of H_2L6'.

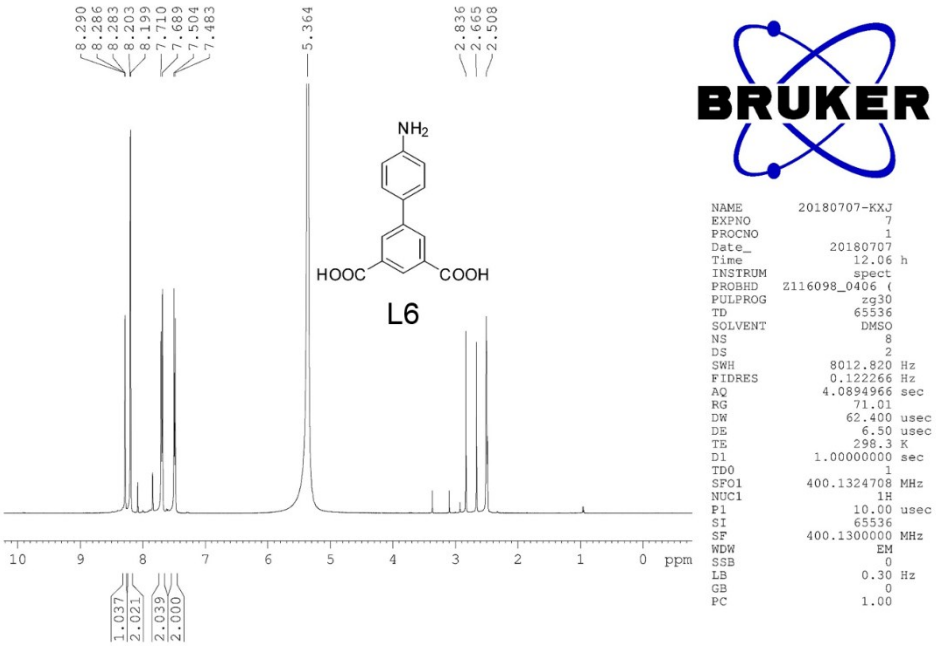

Fig. S20 ^{1}H NMR spectrum of L6.

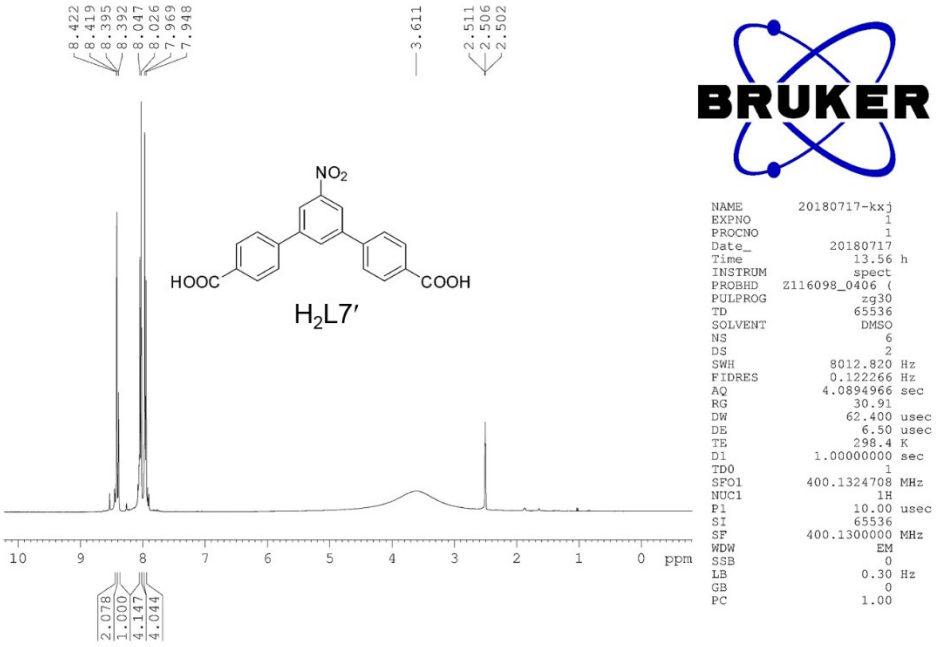

Fig. S21 ^{1}H NMR spectrum of H_2L7'.

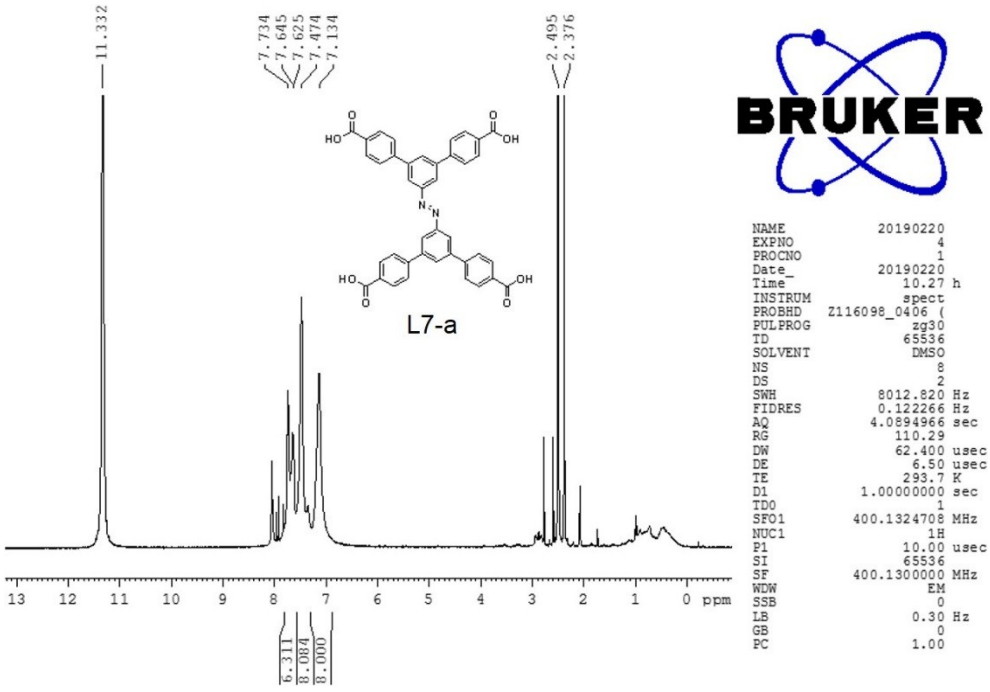

Fig. S22 ^{1}H NMR spectrum of L7-a.

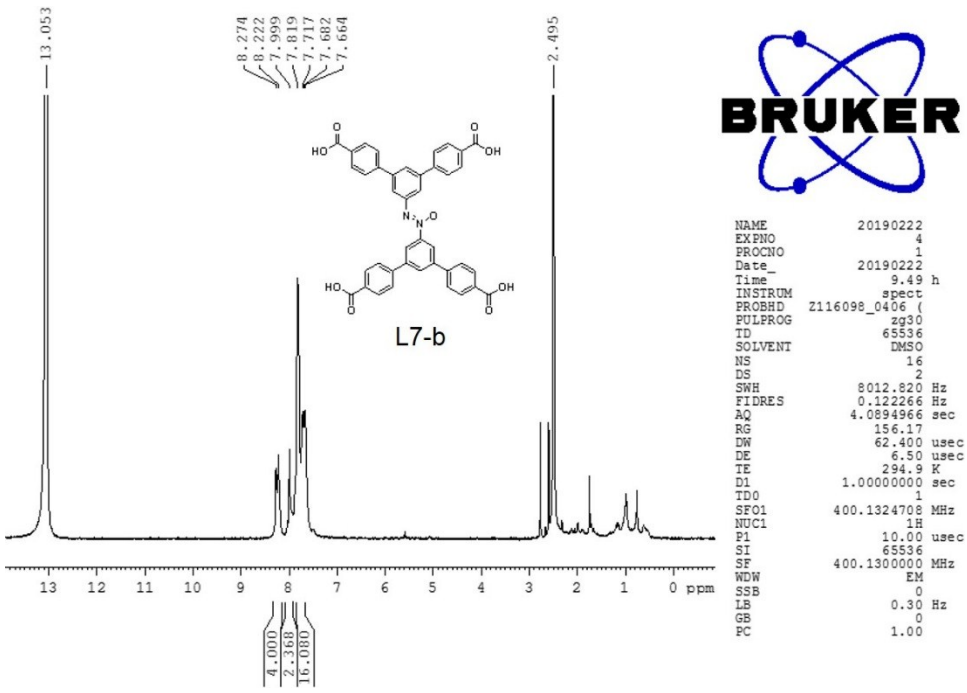

Fig. S23 ^{1}H NMR spectrum of L7-b.

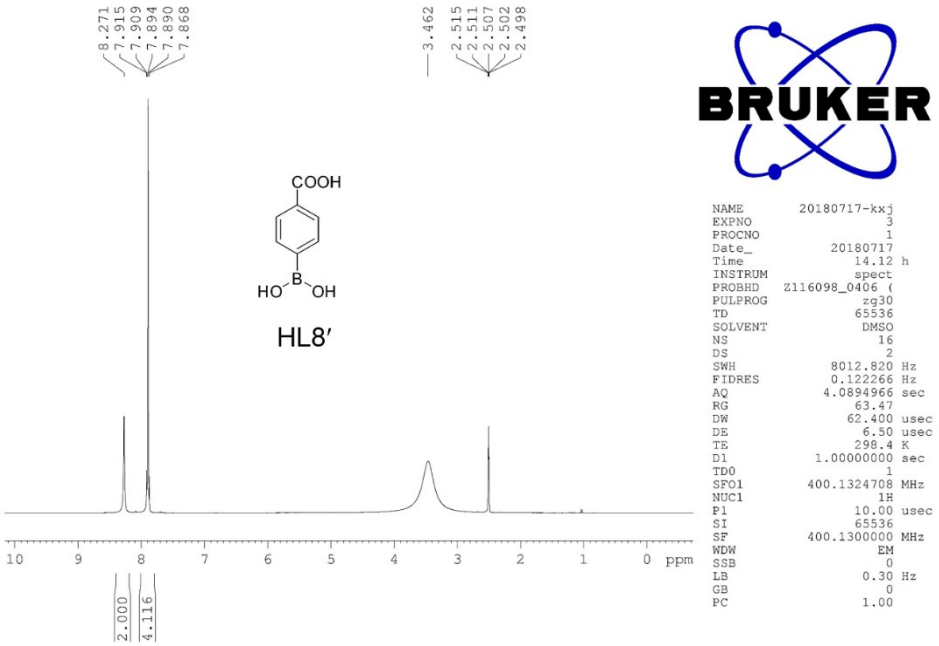

Fig. S24 ^{1}H NMR spectrum of HL8′.

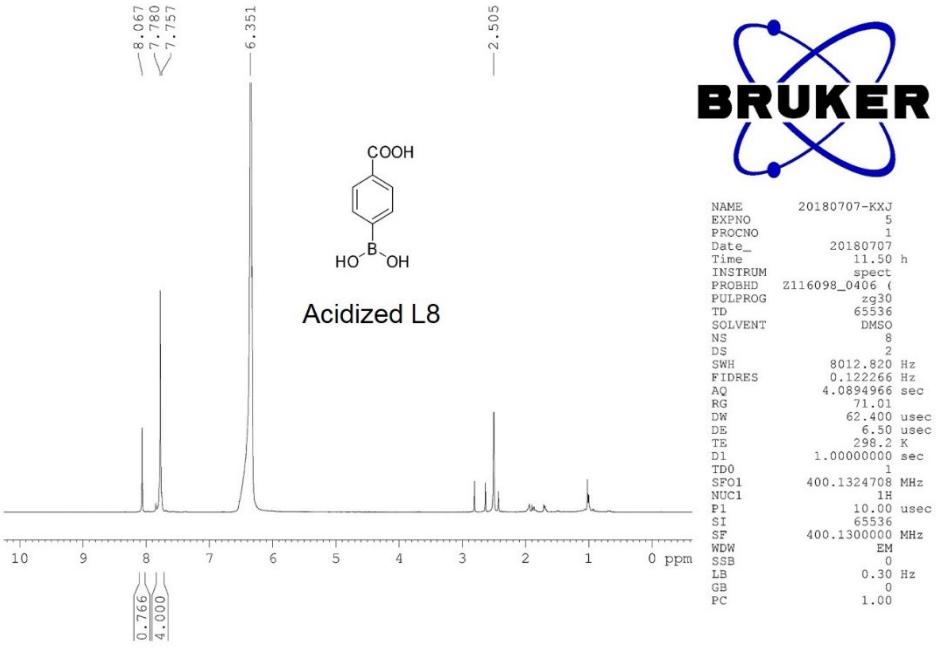

Fig. S25 ^{1}H NMR spectrum of acidized L8.